Multiple Coulomb Excitation of Rotational Levels in Even-Even Nuclei*

J. DE BOER, G. GOLDRING,† AND H. WINKLER
California Institute of Technology, Pasadena, California
(Received 20 January 1964)

An experimental study of excitation probabilities of rotational states with spins 2, 4, 6, and 8 in 22 even-even nuclei in the region $150 \leq A \leq 192$ has been carried out by means of multiple Coulomb excitation with oxygen ions of energies up to 44 MeV. In the region of strong nuclear deformation, the results are in good agreement with excitation probabilities calculated on the basis of the rotational model. It has, however, been observed, that the intrinsic quadrupole moment Q_0, derived from the observed excitation probabilities, increases for higher rotational states, especially in the transition region. For Sm^{152}, the dependence of the probabilities for excitation of the 2^+ and 4^+ states on the bombarding energy are compared with calculations based on higher order perturbation theory and on multiple Coulomb-excitation theory. In the nuclei Sm^{152}, Gd^{160}, W^{186}, Os^{188}, and Os^{192}, nonrotational transitions were observed. The excitation probabilities of the second excited 2^+ states are compared with the predictions of the Davydov model.

I. INTRODUCTION

THE electric quadrupole transition probabilities between the ground state and the lowest excited states of most nuclei have been determined by Coulomb excitation. If light particles (protons, deuterons, alpha particles) are used as projectiles, the excitation probability is usually so small that a first-order perturbation calculation describes the process quite accurately.[1] For heavy ions of sufficiently high bombarding energies, however, the excitation probability can become comparable to unity and the perturbation treatment breaks down. In an intermediate situation, higher than first-order perturbation expansions may be used which involve an increasingly larger number of parameters, and the calculation of the process becomes more and more complex. The sudden approximation[2–4] avoids the perturbation expansion but has instead to assume a model for the nucleus which gives all the nuclear quantities used in the calculations in terms of a small number of parameters, which are characteristic for the particular nuclear model.

The Coulomb excitation of a symmetric rotator is described by two parameters, namely the moment of inertia $\Im$ which gives the energy spectrum as

$$E_I = E_0 + (\hbar^2/2\Im) I(I+1) \tag{1}$$

and the intrinsic quadrupole moment Q_0 which gives the $B(E2)$ values and the static quadrupole moments as

$$B(E2, I \rightarrow I+2) = \frac{15}{32\pi} e^2 Q_0^2 \frac{(I+1)(I+2)}{(2I+1)(2I+3)}, \tag{2}$$

$$Q_I = -Q_0 I/(2I+3); \quad I = 0, 2, 4, \cdots. \tag{3}$$

For nuclei whose proton and neutron numbers are both far from closed-shell numbers, the energies and spin sequence of the lowest states are fairly accurately given by Eq. (1). Deviation from Eq. (1) can approximately be expressed in terms of a parameter B, defined by

$$E_I - E_0 = (\hbar^2/2\Im) I(I+1) - B[I(I+1)]^2. \tag{4}$$

The value of B, determined from the energies of the 4^+ levels is found to be of the order of $\hbar^2/2\Im \times 10^{-3}$ for even-even nuclei with $154 \leq A \leq 180$. (See also Fig. 11.)

Much less information is available on the static and dynamic electric quadrupole moments of these nuclei. Double Coulomb-excitation experiments[5] and measurements of the lifetimes of 4^+ rotational states[6] have shown that the $B(E2)$ ratios for the transitions $4^+ \rightarrow 2^+$ and $2^+ \rightarrow 0^+$ are correctly given by Eq. (2).

The present work was performed in order to obtain systematic information on the higher rotational states of strongly deformed nuclei and on the lowest 2^+ and 4^+ states of nuclei in the transition region between strong deformations and closed-shell configurations. Some of the results presented in this work have previously been communicated.[7,8] Small differences between the results given in Refs. 7 and 8 and the present ones are mainly due to an improved determination of the efficiencies of the gamma counters. Twenty-two nuclei with $150 \leq A \leq 192$ have been Coulomb-excited with oxygen ions of 18–44 MeV. The results are analyzed in terms of calculations by Alder and Winther, in which the sudden approximation is applied to the rotational model.

* Supported in part by the U. S. Atomic Energy Commission and in part by the Office of Naval Research.
† Present address: The Weizmann Institute of Science, Rehovoth, Israel.
[1] K. Alder, A. Bohr, T. Huus, B. Mottelson, and A. Winther, Rev. Mod. Phys. **28**, 432 (1956).
[2] K. Alder and A. Winther, Kgl. Danske Videnskab. Selskab, Mat. Fys. Medd. **32**, No. 8 (1960).
[3] K. Alder, in *Proceedings of the Third Conference on the Reactions between Complex Nuclei, Asilomar, California, 1963* (University of California Press, Berkeley and Los Angeles, 1963), p. 253; and private communication.
[4] K. Alder, W. Bierter, M. Simonius, and A. Zwicky (private communication).
[5] R. Graetzer and E. M. Bernstein, Phys. Rev. **129**, 1772 (1963).
[6] A. C. Li and A. Schwarzschild, Phys. Rev. **129**, 2664 (1963).
[7] G. Goldring, J. de Boer, and H. Winkler, in *Proceedings of the Third Conference on the Reactions between Complex Nuclei, Asilomar, California, 1963* (University of California Press, Berkeley and Los Angeles, 1963), p. 278.
[8] J. de Boer, G. Goldring and H. Winkler, in *Proceedings of the Third Conference on the Reactions between Complex Nuclei, Asilomar, California* (University of California Press, Berkeley and Los Angeles, 1963), p. 317.

Several transitions which do not belong to the ground-state rotational band were observed in Sm^{152}, Gd^{160}, W^{186}, Os^{188}, and Os^{192}. The excitation probabilities for these nonrotational transitions are analyzed in terms of second-order perturbation calculations for the Coulomb-excitation process. For Gd^{160}, W^{186}, Os^{188}, and Os^{192}, the $B(E2)$ values, extracted from this analysis, are compared to the theory of Davydov-Filippov[9] for a nonaxially symmetric rotator.

The Coulomb-excitation process was studied by observing the gamma radiation depopulating the rotational levels. The gamma spectra were recorded in coincidence with projectiles backscattered from the target.

II. EXPERIMENTAL PROCEDURE

A. Apparatus

The experiments described here were performed with the ONR-CIT tandem accelerator. For the beam production, the same procedure as the one described by Graetzer and Bernstein[5] was used and similar performances were achieved.

The energy of the incident beam is known to 0.2%. The bombarding energy is obtained by subtracting the mean energy loss of the oxygen ions in the thin targets, assuming a value of 3 MeV mg^{-1} cm^2.[10] This correction was always smaller than 300 keV.

A schematic view of the setup is shown in Fig. 1. The beam, collimated to 1 mm diam, passes through the hole in an annular shaped solid-state counter of 8-mm-outside and 4-mm-inside diameter. The target is placed at about 7 mm from the counter surface, so that the counter accepts oxygen ions, backscattered through $152°<\theta<165°$. The spectrum seen by the ring counter is shown in Fig. 2 for 31-MeV oxygen ions impinging on a 70-$\mu g/cm^2$ Sm^{152} target evaporated onto a 1000-Å nickel foil. The width of the peaks of about 1 MeV arises from the combined effects of the energy loss in the target and the kinematic spread. The peak comprises elastic scattering and all significant inelastic

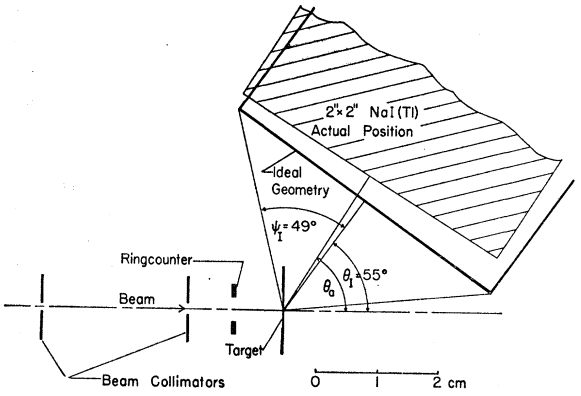

FIG. 1. Schematic view of the apparatus. The beam passes through the hole in an annular shaped solid-state detector which accepts particles backscattered through $152°<\theta<165°$. The NaI counter is placed at such an angle with respect to the beam and at such a distance from the target as to average out the angular distributions of the de-excitation gamma rays (see text).

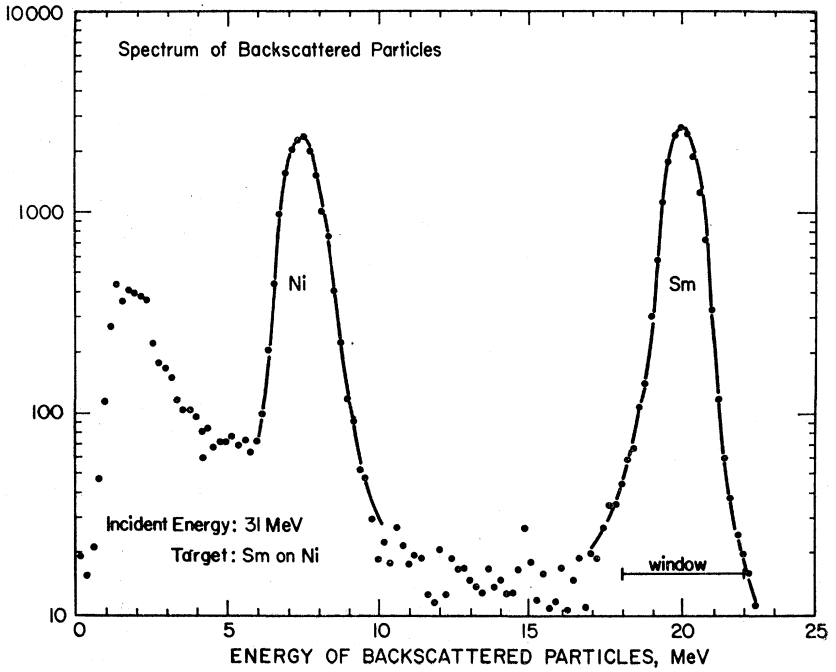

FIG. 2. Energy spectrum of the backward scattered oxygen ions. The window is set so as to accept only ions backscattered from the target material.

[9] A. S. Davydov and G. F. Filippov, Nucl. Phys. 8, 237 (1958).
[10] L. C. Northcliffe (unpublished).

scattering processes. A positive potential of about 300 V was applied to the target. Without this precaution, the performance of the solid-state detector was found to deteriorate (high noise, slow rise time, smaller pulses) within a counting period of about one hour.

The gamma-ray detector consists of a cylindrically symmetric 2-in.×2-in. NaI crystal placed so that its symmetry axis goes through the beam spot on the target and forms an angle φ of about 58° with respect to the beam direction. The distance is such, that the opening angle 2ψ for gamma rays hitting the front face of the crystal is about 86°. With this geometry, the fraction of gamma rays seen by the crystal is almost independent of the (strongly anisotropic) angular distributions of the gamma rays. The solid angle subtended by the counter is about 10% of the whole sphere. For the runs on osmium and on Sm^{150}, a 3-in. ×3-in. sodium-iodide crystal was used in a similar geometry.

B. Targets

The targets were prepared by vacuum-evaporation of 5–20 mg of the isotopically enriched material onto nickel backings of about 1000-Å thickness. The high temperatures required for the evaporation of rare-earth oxides were obtained by electron bombardment of small quantities of the samples contained in carbon crucibles of 1.5–3 mm diameter.[11] Most targets had a thickness of about 100 $\mu g/cm^2$. Osmium targets turned out to be very difficult to produce in adequate thicknesses, the thickest being less than 1 $\mu g/cm^2$.

The use of thin targets avoids overloading of the junction detector which is sensitive to high counting rates[12] and also gives an energy definition of the bombarding particles close to the energy definition of the accelerator.

C. Gamma-Ray Angular Distributions

Because of the $E2$ nature of all transitions involved, and the symmetry of the particle counter around the beam axes, the gamma angular distribution can be written in the form

$$W(\Omega)=1+A_2P_2(\cos\Omega)+A_4P_4(\cos\Omega), \quad (5)$$

where Ω is the angle between the direction of emission of the gamma ray and the incident beam. The counting rate, measured by a counter of finite angular aperture 2ψ and position φ can be written in the form

$$W(\varphi,\psi,E_\gamma;A_2,A_4)=1+\epsilon_2(\psi E_\gamma)\times A_2\times P_2(\cos\varphi) +\epsilon_4(\psi E_\gamma)\times A_4\times P_4(\cos\varphi), \quad (6)$$

where ϵ_2 and ϵ_4 depend only on the angular opening 2ψ and on the gamma energy E_γ. If $\varphi=\varphi_I=55°$ then $P_2(\cos\varphi_I)=0$ and W is independent of A_2 for all ψ and E_γ. The opening ψ can now be chosen in such a way that $\epsilon_4=0$ for one particular E_γ. Gamma rays of sufficiently low energy are all counted in the front face of the crystal. In this case, $\epsilon_4=0$ for $\psi=\psi_I=49°$ and W is independent of A_4 for all φ.

This "ideal geometry" could not exactly be realized in our apparatus, because it would have brought the edge of the scintillator housing too close to the beam (see Fig. 1). In the "actual position," a compromise was made by taking $\varphi=\varphi_a=58.5°$ and $\psi=\psi_a=43°$. In this geometry, P_2 has a value of -0.09. The magnitude of $P_4(\varphi_a)\times\epsilon_4(\psi=43°, E_\gamma)$ for the 2-in.×2-in. crystal is estimated to be -0.03 for $E_\gamma<100$ keV, -0.08 for $E_\gamma=200$ keV, -0.14 for $E_\gamma=300$ keV, and -0.20 for $E_\gamma=600$ keV. The signs and magnitudes of A_2 and A_4 in formula (5) are such that the contributions due to the P_2 and P_4 terms almost cancel each other. The size of the term $\epsilon_2\times A_2\times P_2+\epsilon_4\times A_4\times P_4$ in Eq. (6) is estimated to be less than 0.05 for the deexcitation of a 2^+ state and less than 0.02 for all other transitions.

D. Evaluation of Coincidence Spectra

The pulses from the photomultiplier, gated by the output of a fast-slow coincidence system, were analyzed in a multichannel kicksorter. The occurrence of a gate signal required a coincidence between any multiplier pulse and a pulse from the particle counter corresponding to an oxygen ion backscattered from the target nucleus. The resolving time 2τ of the fast coincidence system was set to 48 nsec to ensure 100% coincidence efficiency for all gamma-ray energies between 50 and 500 keV. Examples of coincidence spectra are given in Figs. 3, 4, and 8–11.

In order to obtain the number of gamma rays emitted per backscattered oxygen ion from the areas under the photopeaks in the coincidence spectra, the efficiencies of the counters were determined by placing calibrated sources at the location of the beam spot on the target. This calibration is believed to be accurate to about 8%. In the runs with high bombarding energies, a Cu+Sn absorber was placed between target and gamma counter. This absorber served two purposes. First it reduced the counting rate in the K x-ray peak and in the $2^+\rightarrow 0^+$ transition by a factor of 10–20 so that the pileup of pulses was appreciably reduced. Second, the absorber almost eliminates the sum peak, which occurs when both members of a gamma cascade depopulating the 4^+ state are counted in the NaI crystal. According to the $I(I+1)$ rule, the energy of this sum peak is 10/11 of the energy of the $6^+\rightarrow 4^+$ transition. (Compare Figs. 4 and 11.) The uncertainty in the attenuation factor made it impossible to obtain accurate values of the $2^+\rightarrow 0^+$ intensities in the runs in which absorbers were used.

The number of gamma rays per backscattered oxygen ion was finally obtained by applying corrections for the fractional dead time of the multichannel analyzer, for random coincidences, for counting losses

[11] Y. Dar, H. M. Loebenstein, and J. de Boer, Nucl. Instr. Methods (to be published).

[12] D. Eccleshall, B. M. Hinds, and M. J. L. Yates, Nucl. Phys. 32, 190 (1962).

in the scaler monitoring the number of backscattered particles, for Compton-tails of higher lines and for the loss of counts due to the addition of simultaneous members of a cascade into the sum peak. From this number, the number of de-excitations was derived by taking into account internal conversion. The K and L conversion coefficients were taken from the tables of Sliv and Band[13] and the contributions of the higher shells were accounted for by adding $\frac{1}{3}$ of the L coefficient.

We define the de-excitation probability R_I as

$$R_I=\frac{\text{number of de-excitations of a level with spin } I}{\text{number of backscattered particles}}. \tag{7}$$

For rotational levels in even-even nuclei, which decay by $E2$ cascades only, the transition $I\rightarrow I-2$ will occur whenever a level with spin $J\geq I$ has been excited. We therefore have

$$R_I=\sum_{J\geq I} P_J, \tag{8}$$

where P_J denotes the probability for Coulomb excitation of a level with spin J. The excitation probabilities are normalized so that

$$\sum_{J=0}^{\infty} P_J=1. \tag{9}$$

The probabilities R_I, calculated from the theoretical values for P_J, are the quantities that are compared with the experiment in the present analysis.

III. EXCITATION FUNCTIONS FOR Sm^{152}

The first group of experiments consists of a series of precision measurements on Sm^{152} for a wide range of bombarding energies, in order to study the dependence of the Coulomb-excitation probabilities on the excitation parameters.

A. Coincidence Spectra

Examples of coincidence gamma spectra from the bombardment of Sm^{152} with 18- and 42-MeV oxygen ions are shown in Figs. 3 and 4. The prominent peaks

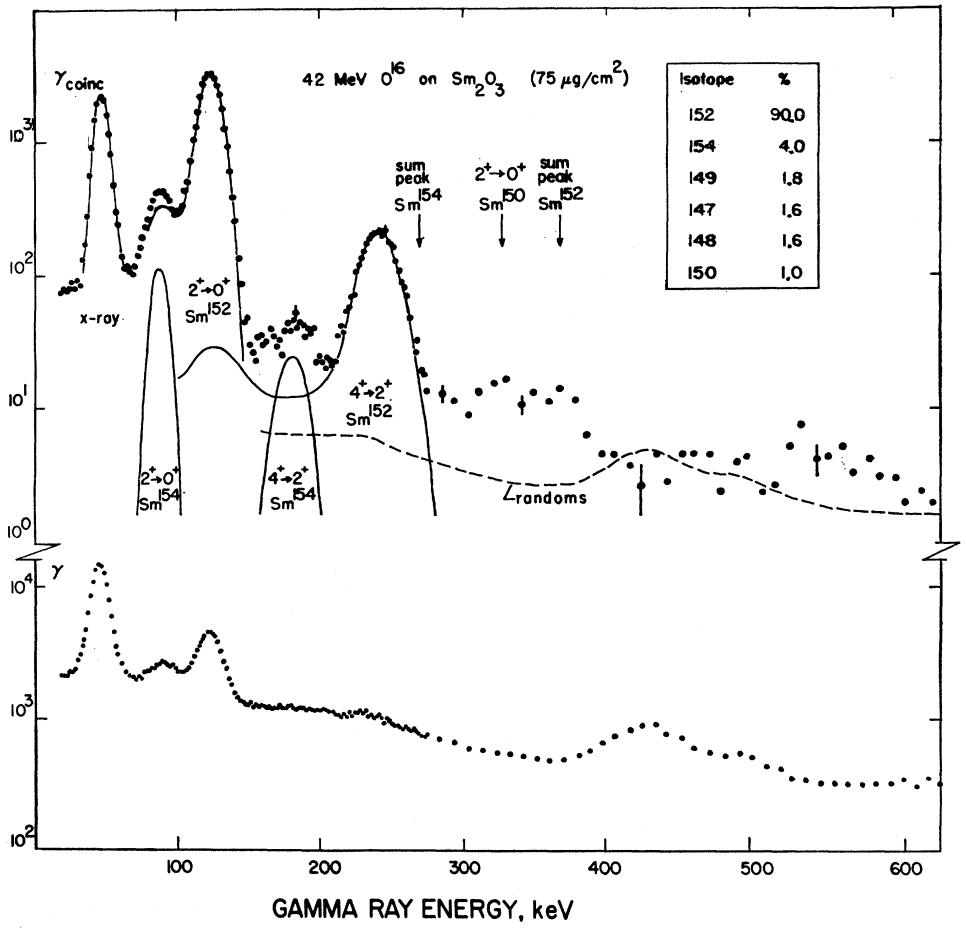

FIG. 3. Spectrum of gamma rays from Sm^{152} at 42-MeV bombarding energy. The upper part shows the spectrum in coincidence with backscattered oxygen ions and the lower half shows the ungated spectrum. For the higher gamma energies, the average number of coincidence counts in 5 or 10 channels is plotted. The contributions from the isotopic impurities in the sample are also indicated. The random spectrum, indicated by a dashed line, has the same shape as the ungated spectrum.

[13] L. A. Sliv and M. I. Band, *Coefficients for Internal Conversion of Gamma Radiation* (Academy of Sciences of the USSR, Moscow, 1956, 1958), Parts I and II.

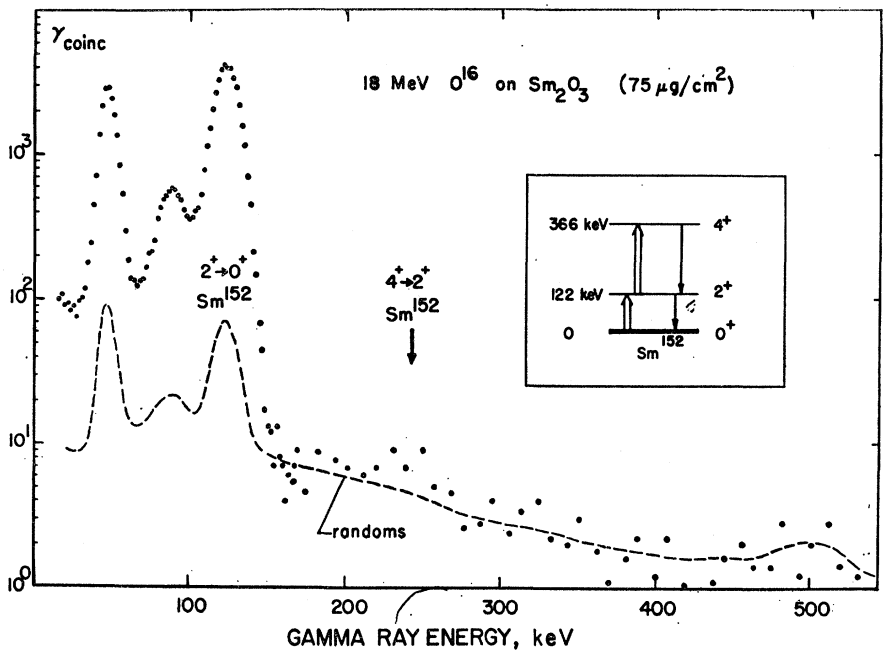

FIG. 4. Coincidence spectrum of gamma rays from Sm^{152} at 18-MeV bombarding energy. The two most prominent peaks are the K x-ray and the $2^+ \rightarrow 0^+$ transition in Sm^{152}. A peak corresponding to the $2^+ \rightarrow 0^+$ transition in Sm^{154} is visible. At 244 keV, an indication of the $4^+ \rightarrow 2^+$ transition can be seen. The dashed line shows the random coincidences.

are due to K x rays and gamma rays of 122 and 245 keV from the $2^+ \rightarrow 0^+$ and $4^+ \rightarrow 2^+$ transitions in Sm^{152}. In the lower part of Fig. 3, the singles gamma spectrum is shown for the same bombarding conditions. The spectrum of the random coincidences, indicated by a dashed line in the coincidence spectrum, was found to have the same shape as the singles spectrum. Almost all counts in the coincidence spectra can be assigned to Coulomb excitation of Sm^{152} and its isotopic impurities. The random coincidences which range to high gamma-ray energies, are probably due to nuclear reactions of the projectiles with the nickel backing and light elements in the target.

B. Excitation Parameters and Experimental Results

The experimental values of the excitation probabilities for Sm^{152} are listed in Table I. The first column gives the bombarding energy, reduced by the mean energy loss of the oxygens in the target (about 80 keV for the Sm^{152} target). The next two columns list the Coulomb excitation parameters ξ and χ, defined by

$$\xi_{if}=\frac{Z_1Z_2A_1^{1/2}(1+A_1/A_2)\Delta E_{if}}{12.65E^{3/2}}, \quad (10)$$

and

$$\chi_{i\rightarrow f}=14.36\frac{\pm[B(E2;i\rightarrow f)]^{1/2}\times A_1^{1/2}}{(1+A_1/A_2)^2Z_1Z_2^2}E^{3/2}. \quad (11)$$

The indices 1 and 2 refer to projectiles and target nucleus, respectively. The charge numbers are denoted by Z. The laboratory energy E and the transition energy ΔE_{if} are both measured in MeV, the reduced transition probability $B(E2)$ in $e^2\times10^{-48}$ cm^4 and the masses A in amu.[14] The sign of $[B(E2, i\rightarrow f)]^{1/2}$ is to be the same as the sign of the reduced matrix element $\langle i||E2||f\rangle$. For the calculation of the adiabaticity parameter ξ, ΔE is taken as the energy of the $2^+ \rightarrow 0^+$ transition. The parameter $\chi_{0\rightarrow2}$ is the transition amplitude for a $0^+ \rightarrow 2^+$ transition in first-order perturbation theory for $\xi=0$ and $\theta=180°$. The χ values, given in column 2 of Table I, are calculated for $B(E2)=3.43$, a weighted average[15] of previous determinations of this quantity. The last two columns list the experimentally determined values for R_2 and R_4. The uncertainties in the absolute efficiencies of the gamma counter, which

TABLE I. Results of the precision measurements of the probabilities for Coulomb excitation of the 2^+ and 4^+ rotational states in Sm^{152}. ξ and χ are excitation parameters defined by Eqs. (10) and (11). The value of the bombarding energy E is known to $\pm0.2\%$. The values R_2 and R_4 are the experimental probabilities for observing the decay of the 2^+ and 4^+ rotational states, respectively, in a collision in which the oxygen ion was backscattered. The uncertainty in the efficiency of the gamma counter is absorbed in the constants K and F. $K=1.00\pm0.08$ and $F=1.00\pm0.08$.

E MeV	$\chi_{0\rightarrow2}$	$\xi_{2\rightarrow0}$	$R_{2\,exp}$	$R_{4\,exp}$
17.94	0.216	0.277	$K\times0.0236\pm0.0004$	$F\times0.000048\pm0.000015$
23.06	0.315	0.190	$K\times0.0645\pm0.001$	$F\times0.00048\pm0.00005$
28.07	0.423	0.141	$K\times0.1305\pm0.001$	$F\times0.00247\pm0.00015$
31.15	0.494	0.121	$K\times0.182\pm0.002$	$F\times0.00525\pm0.00015$
32.95	0.537	0.111	$K\times0.216\pm0.002$	$F\times0.0084\pm0.0002$
36.08	0.616	0.097	$K\times0.289\pm0.004$	$F\times0.0152\pm0.0003$
40.46	0.731	0.082	$K\times0.395\pm0.005$	$F\times0.0292\pm0.0006$
42.10	0.776	0.077	$K\times0.426\pm0.005$	$F\times0.0373\pm0.0007$

[14] The numerical factor in relation (11) differs from the one given in Ref. 2 due to a different choice of the mass unit.

[15] E. M. Bernstein and E. Z. Skurnik, Phys. Rev. **121**, 841 (1961).

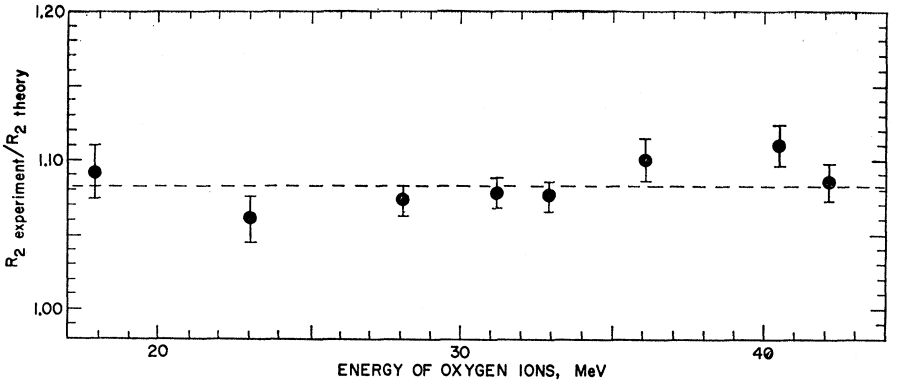

FIG. 5. Comparison of the experimental values from Table I for the de-excitation probability of the 2^+ rotational state in Sm^{152} with the calculations of Ref. 3. The points are consistent with a constant value for $R_{2\,\mathrm{exp}}/R_{2\,\mathrm{theor}}$.

are independent of the bombarding conditions, are absorbed in the constants K and F. The error, quoted for each experimental value, is due to the errors in the corrections, the statistical error and the uncertainty in the position of the beam spot. (In Ref. 7, this last source of error was not taken into account.)

In Figs. 5 and 6, the experimental values are compared with theoretical calculations of the multiple Coulomb excitation of rotational bands. In Refs. 2 and 16, P_I is given for $\xi=0$ and $\theta=180°$ as a function of q which is related to $\chi_{0\to 2}$ by the expression

$$q=(45/16)^{1/2}\times\chi_{0\to 2}. \tag{12}$$

More recently, Alder[3] has calculated $P_I(q, \xi\neq 0, \theta=180°)$. The theoretical values, which were used in the comparison of Figs. 5 and 6, are based on these calculations. The dependence on the deflection angle $\theta\neq 180°$ was taken into account by using an "effective" value for χ or q [see Ref. 2, formula (5.15)]. For the geometry used in this experiment

$$\chi_{\mathrm{eff}}(\theta)=0.965\chi(180°). \tag{13}$$

For backward scattered particles ($\theta\approx 160°$) this approximation is expected to yield quite accurate theoretical values (see Ref. 2, pp. 14, 15). The accuracy may be estimated by comparing the values, obtained by the χ_{eff} approximation with calculations by Alder *et al.*,[4] in which the exact dependence of P_I on θ was taken into account for $\xi=0$. The deviations between the two calculations are smaller than 0.5% for all χ values encountered in the present experiments. For $\xi\neq 0$, the deviations are somewhat larger.

From the comparison in Fig. 5 it can be seen that the experimental dependence of $R_2=1-P_0$ on the bombarding energy is very well reproduced by the theory. In Fig. 6, the de-excitation probability of the 4^+ state in Sm^{152} is compared with the calculation of Ref. 3. The theoretical values for the solid points in

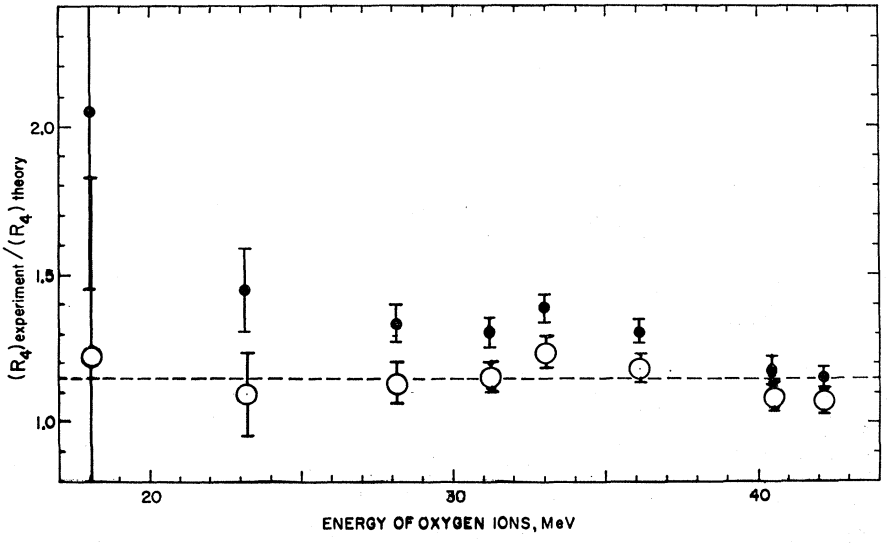

FIG. 6. Comparison of the experimental values from Table I for the de-excitation probability of the 4^+ state in Sm^{152} with the calculations of Ref. 3. For the solid points, ξ values corresponding to the moment of inertia representing the $2\to 0$ transition energy were employed in the calculations of the theoretical values. The open circles were calculated for a moment of inertia that represents the $4^+\to 2^+$ transition energies. The open circles are consistent with a constant value for $R_{4\,\mathrm{exp}}/R_{4\,\mathrm{theor}}$.

[16] R. Graetzer, R. Hooverman and E. M. Bernstein, Nucl. Phys. **39**, 124 (1962).

Fig. 6 were obtained by taking $\xi=\xi_{2\to0}$. If, however, a ξ value is used that corresponds to a moment of inertia which reproduces the experimentally determined transition energy $\Delta E_{4\to2}$ rather than $\Delta E_{2\to0}$ (see discussion below) the points marked by open circles are obtained. These points, which have the same experimental error as the solid ones, are consistent with a horizontal line in Fig. 6.

C. Higher Order Perturbation

In Ref. 7 it was attempted to relate the dependence of R_2 on E to the magnitude of the static quadrupole moment of the 2^+ state. Theoretically, the dependence of the Coulomb-excitation probability on Q_{2^+} can be calculated, if higher than first-order perturbation expansions are used. This "reorientation effect" has been considered by various authors.[17–19] Lin and Masso[19] have pointed out that in the case of Sm^{152}, the bombarding energies must be very low in order to prevent the higher than second-order terms in the perturbation expansion from being comparable in size to the reorientation effect,[20] so that the present experiments are not conclusive in this respect. The situation is illustrated in Fig. 7. The contributions of the second-order terms in the perturbation expansion were calculated using the tables of Douglas.[21] The ratios $P_2^{(12)}/P_2^{(11)}$, $(P_2^{(12)}+P_2^{(22)})/P_2^{(11)}$ and $P_2^{(S)}/P_2^{(11)}$ are plotted as a function of the bombarding energy E for Sm^{152} and for $\theta=160°$. The symbols $P^{(11)}$ and $P^{(22)}$ denote the excitation probabilities in first and second order, $P^{(12)}$ is the interference between first and second order and $P^{(S)}$ is the excitation probability in the calculation of Ref. 3. The numerical formulas for these probabilities are

$$P_2^{(11)}=17.90\chi_{0\to2}{}^2\times\sin^4(\theta/2)\times df(\xi,\theta)/d\Omega, \tag{14}$$

$$P_2^{(12)}=9.49\chi_{0\to2}{}^3\times\frac{\langle2||E2||2\rangle}{[B(E2;\,0\to2)]^{1/2}}\times\{(\tfrac{3}{2})^{1/2}[I_{22}(\xi,\theta)\beta_{2-2}(2,2,\xi,0,\theta)+I_{2-2}(\xi,\theta)\beta_{22}(2,2,\xi,0,\theta)]-I_{20}(\xi,\theta)\beta_{20}(2,2,\xi,0,\theta)\}, \tag{15}$$

$$P_2^{(22)}=16.03\chi_{0\to24}\times\sin^4(\theta/2)\times\frac{|\langle2||E2||2\rangle|^2}{B(E2,\,0\to2)}\times dF(\xi,0,2,\theta)/d\Omega. \tag{16}$$

In these expressions, $\chi_{0\to2}$ is defined by (11) and $\langle2||E2||2\rangle$ is related to the quadrupole moment of the 2^+ state by

$$eQ_{2^+}=\tfrac{4}{5}(2\pi/7)^{1/2}\langle2||E2||2\rangle. \tag{17}$$

In the rotational model, $\langle2||E2||2\rangle/[B(E2,\,0\to2)]^{1/2}=-(10/7)^{1/2}$. This value was used for the calculations in Fig. 7. The functions $df/d\Omega$ and I are tabulated in Ref. 1 and β and $dF/d\Omega$ are given in Ref. 21.

From Fig. 7 it can be seen that for energies higher than 22 MeV, $P_2^{(12)}$ accounts for less than half of the difference between $P_2^{(S)}$ and $P_2^{(11)}$. The measurement of P_2 would have to be extended to very low bombarding energies in order to obtain accurate values for $P_2^{(12)}$, which is proportional to the static quadrupole moment of the 2^+ state. This shows that other terms of order χ^4 (interference between first- and second-order perturbation) are, in this case, more important than $P_2^{(22)}$.

On the other hand the multiple Coulomb-excitation theory of Alder[3] accounts for these higher order effects, provided they all conform to the rotational patterns. The remarkable degree of accuracy with which the theory[3] fits the strong energy dependence of the excitation probabilities (Figs. 5 and 6, Table I) shows that the set of nuclear quantities, given by the rotational model, describes the multiple process well. In order to assess the accuracy with which a specific nuclear quantity may be determined in this way, we have to

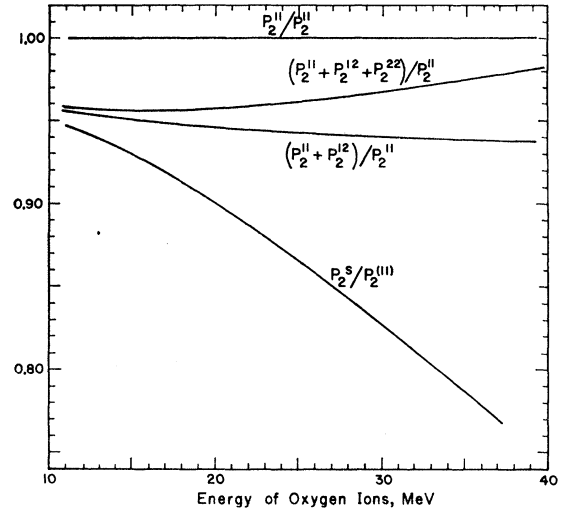

FIG. 7. Perturbation calculations and diagonalization calculations of the excitation probability P_2 of the 2^+ state in Sm^{152}. All probabilities are given relative to the first order perturbation treatment. P^{11} and P^{22} denote first- and second-order perturbation, respectively, and P^{12} denotes the interference term between first and second order. P^S is the excitation probability calculated by the diagonalization method of Ref. 3.

[17] G. Breit, R. L. Gluckstern and J. E. Russell, Phys. Rev. **103**, 727 (1956); **105**, 1121 (1957).
[18] D. Beder, Phys. Letters **3**, 206 (1963); Can. J. Phys. **41**, 547 (1963).
[19] D. L. Lin and J. F. Masso, in *Proceedings of the Third Conference on the Reactions between Complex Nuclei, Asilomar, California, 1963* (University of California Press, Berkeley and Los Angeles, 1963), p. 267.
[20] From the work by J. Eichler, Phys. Rev. **133**, B1162 (1964), it follows that the effects due to virtual $E1$ transitions are negligible in this case.
[21] A. C. Douglas, Nucl. Phys. **42**, 428 (1963) and Atomic Weapons Research Establishment Report NR/P-2/62, Aldermaston, England (unpublished).

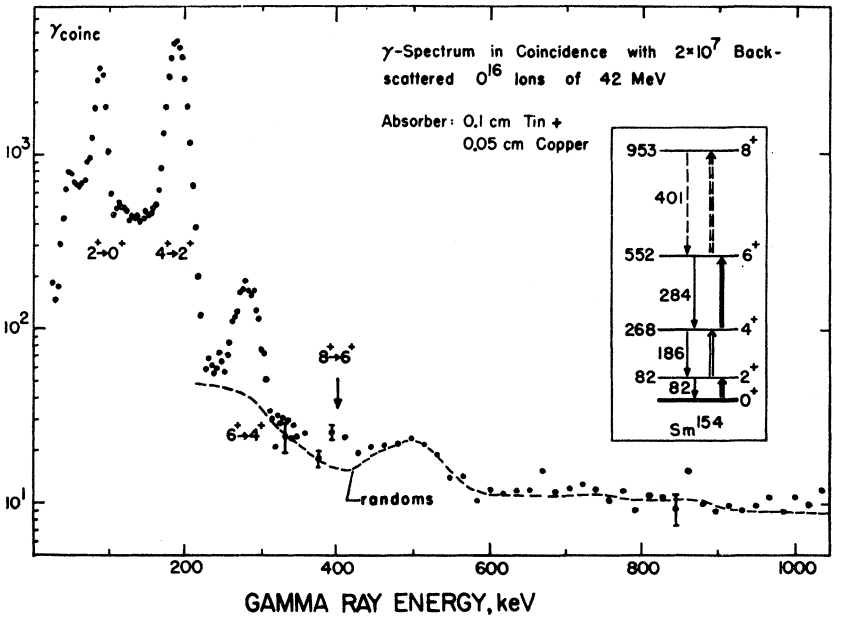

FIG. 8. Coincidence gamma spectrum of Sm^{154}. The peaks corresponding to the $2^+ \rightarrow 0^+$ and $4^+ \rightarrow 2^+$ transitions are attenuated with an absorber by factors of 12 and 1.5, respectively. The assignment of the weak line at $\approx$401 keV as the $8^+ \rightarrow 6^+$ transition is based on the energy and intensity of the gamma ray and on the fact that it disappears at lower bombarding energies.

know how sensitively the calculations depend on each quantity. Such calculations are, however, not yet available.

IV. DEFORMED EVEN-EVEN NUCLEI

A. Coincidence Spectra

This group of experiments deals with a large number of nuclei in the region of stable equilibrium deformation. Examples of coincidence gamma-ray spectra are given in Figs. 8–11. The nuclei in the region of strong deformation ($154 \leq A \leq 180$) all have similar rotational parameters and therefore exhibit similar spectra. The strong dependence of the Coulomb-excitation probabilities on Z_2, the charge number of the target, is illustrated in Figs. 8 and 9. Peaks corresponding to the first, second, and third rotational transitions can clearly be seen. Compared to $_{62}Sm_{92}^{154}$, the coincidence spectrum for $_{72}Hf_{106}^{178}$ shows a much weaker $6^+ \rightarrow 4^+$ transition. The assignment of the weak line at 401 keV in the Sm^{154} spectrum as the $8^+ \rightarrow 6^+$ transition is based on the energy and intensity of the gamma ray and on the fact that it disappears at lower bombarding energies.

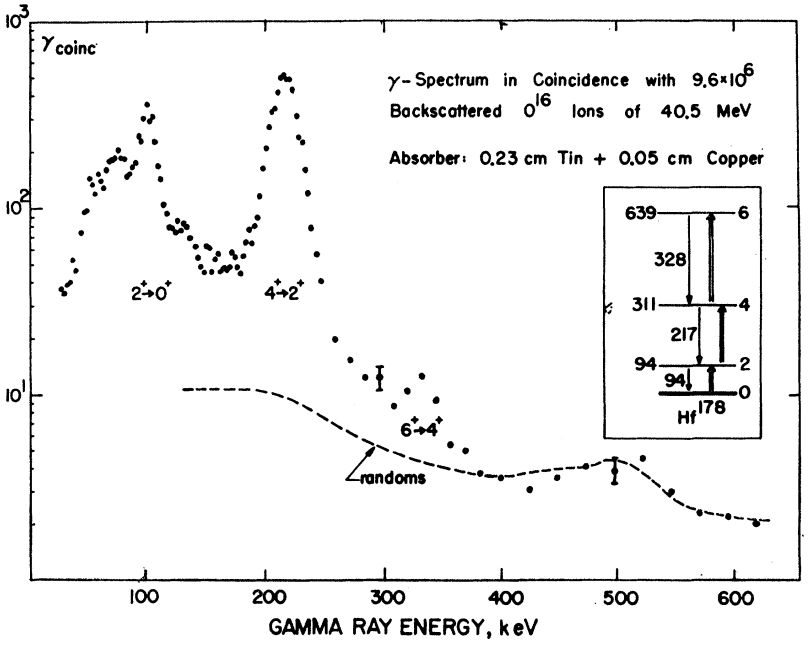

FIG. 9. Coincidence gamma spectrum of Hf^{178}. The peak corresponding to the $2^+ \rightarrow 0^+$ transition is attenuated by a factor of 24.

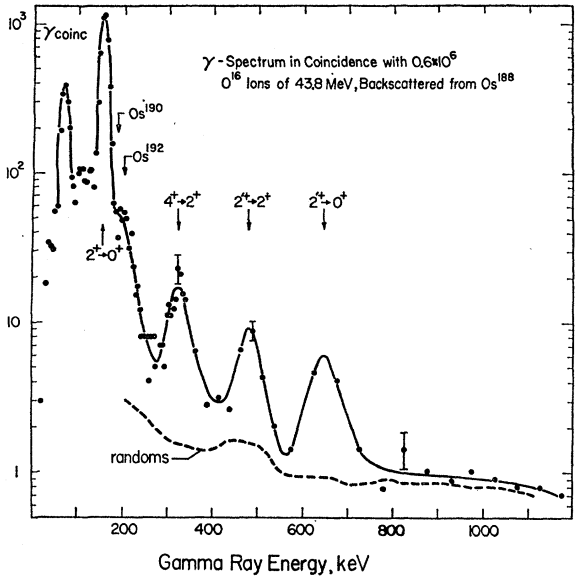

FIG. 10. Coincidence gamma spectrum of Os^{188}. In addition to the rotational transitions, the $2'^{+} \rightarrow 0^{+}$ and the $2'^{+} \rightarrow 2^{+}$ peaks can be seen.

The spectrum of Os^{188} is shown in Fig. 10 as an example of a nucleus in the transition region between spheroidal and spherical equilibrium shape. The transitions corresponding to the cascade and crossover decay of the second 2^{+} state have intensities which are comparable to the intensity of the $4^{+} \rightarrow 2^{+}$ transition.

In Fig. 11, the coincidence spectrum from Sm^{152} bombarded with 43.1-MeV oxygen is shown. The effect of the gamma absorber in reducing the intensity of the sum peak can be seen by comparison with Fig. 3. The prominent peak at 550 keV is assigned to the $0'^{+} \rightarrow 2^{+}$ transition. The isotopic impurities that show up in Fig. 3, are not visible in Fig. 11 because a 99% enriched sample was used for this run.

Except for osmium, where the thinness of the targets required extremely long exposure times, each target has been bombarded with oxygen ions of at least two different energies in order to confirm the multiplicity of the $E2$ excitation process assumed by the rotational description. For the lowest bombarding energies, the spectra were usually taken without a gamma absorber so that the intensities of the $2^{+} \rightarrow 0^{+}$ and $4^{+} \rightarrow 2^{+}$ transitions could be determined. At the higher bombarding energies, the use of absorbers was necessary in order to determine the energies and intensities of the $6^{+} \rightarrow 4^{+}$ transitions without contributions from the sum peaks.

B. Energies of Rotational Transitions

The transition energies, determined in our experiments, are listed in Table II. They are in good agreement with energy determinations by other investigators. From a fit of the weighted averages of the level energies with an expression of the form (4) the values of $B \times 2\mathfrak{I}/\hbar^2$ have been determined and are plotted in Fig. 12 as a function of the mass number. We can see from Fig. 12 that deviations from the $I(I+1)$ rule [Eq. (1)] are encountered. They are particularly large in the transition region ($A \approx 150$ and $A \gtrsim 188$).

Alternatively, the experimental energy values can be fitted with a formula of type (1) if an effective moment of inertia $\mathfrak{I}_{\text{eff}}(I-2 \rightarrow I)$ is introduced for each transition. Because B in (4) is positive, $\mathfrak{I}_{\text{eff}}$ increases with increasing spin. On the other hand, the theoretical calculations for the multiple Coulomb excitation of a rotational band $P_I(\chi, \xi, \theta=\pi)$ have been carried out[3] for an energy spectrum given by Eq. (1), i.e., a constant value for $\mathfrak{I}$ has been assumed. Thus, all $\xi_{I-2 \rightarrow I}$ values for the higher transitions which enter implicitly in Alder's calculation of P_I, are expressed in terms of $\xi_{0 \rightarrow 2}$ with the help of Eqs. (1) and (10). Since P_I

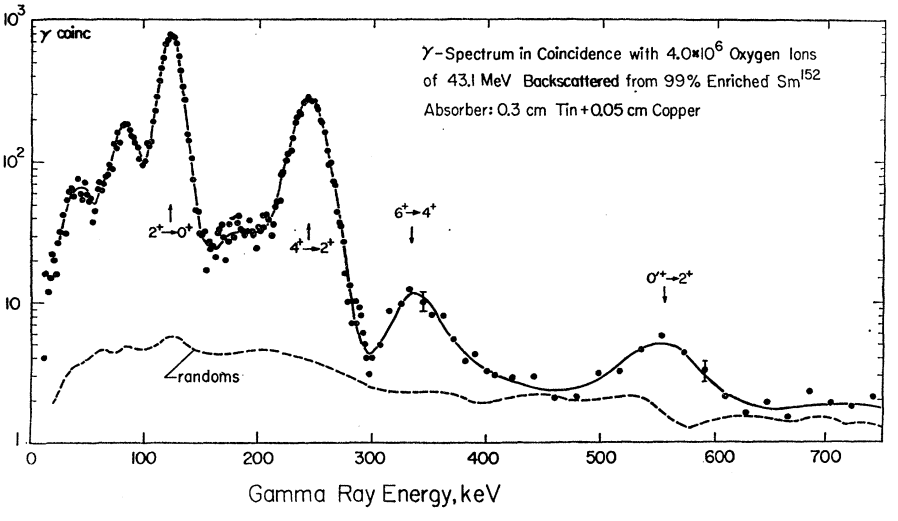

FIG. 11. Coincidence gamma spectrum of Sm^{152}. The use of a gamma-ray absorber eliminates the sum peak, visible in Fig. 4. The peak at 550 keV is assigned to the $0'^{+} \rightarrow 2^{+}$ transition in Sm^{152}.

depends strongest on the largest transition energy, i.e., the energy $\Delta E_{I-2\to I}$, a value for ξ corresponding to $\Im_{\text{eff}}(I-2\to I)$ has been used in the comparison of theory and experiment. (See also discussion of Fig. 6.) For rotational bands whose $\Im_{\text{eff}}$ increases strongly with I, this consideration is of importance if ξ is large.

C. Results on Rotational Transitions

The measured values of R_I are listed in Table III. The ξ values given in the third column of this table are determined by Eq. (10) from the energy of the $2^+\to 0^+$ transitions. Column 4 lists the value of $\chi_{0\to 2}$ defined by Eq. (11). The $B(E2)$ values used for the calculation of $\chi_{0\to 2}$ were determined by inelastic scattering (Refs. 22 and 23). For the osmium isotopes, where no inelastic scattering data were available, the $B(E2)$ values were determined from the present experiments in such a way as to reproduce the theoretical values[3] for the de-excitation probabilities of the 2^+ states. Columns 6–9 list the de-excitation probabilities R_I for $I=2$, 6, and 8. The number in parenthesis following each experimental value of R_I gives the error in percent of the measured value. In columns 10–13, the ratios of experimental to theoretical values of R_I are given. The theoretical de-excitation probabilities were obtained by interpolation of the tables by Alder[3] which give P_I for $I=2$–8 as a function of χ and ξ and for $\theta=180°$. An effective χ_{eff} was used to account for the dependence on θ [see Eq. (13)]. For the theoretical excitation probability of a state with spin I, a ξ value corresponding to a moment of inertia that represents the energy of the $I\to I-2$ transition was employed.

We notice that the average value of the ratio $R_{2\text{ exp}}/R_{2\text{ theor}}$ is higher than unity. This can have various reasons: (a) The assumed values for $B(E2, 0^+\to 2^+)$ from Refs. 22 and 23 may be too small, (b) the assumed value for the total conversion coefficient $\alpha(2^+\to 0^+)$ may be too high, and (c) the assumed efficiency of the gamma counter may be too low. The discrepancies are, however, too small to allow a definite decision on the basis of the present experiments. The conversion coefficient, required to make $R_{2\text{ exp}}/R_{2\text{ theor}}=1$ would be smaller than the theoretical value of Sliv and Band.[11] Some recent experiments, in particular the work of Fossan and Herskind[24] indicates, however, an experimental value of $\alpha(2^+\to 0^+)$ about 12% larger than the theoretical one. As can be seen from columns 10–13, $R_{I\text{ exp}}/R_{I\text{ theor}}$ is independent of the bombarding energy within the limits of error. This is consistent with the multiple excitation of a rotational state of spin I.

The results are graphically represented in Fig. 13. The solid curves show the calculations of Ref. 3 for $R_I(\chi, \xi, \theta=180°)$; and the broken curve gives $R_I(\chi, \xi=0, \theta=160°)$ of Ref. 4. The experimental values for R_I are plotted as a function of χ, and for four ranges of ξ values, as indicated by different points. The points clearly group into clusters corresponding to the respective rotational states.

TABLE II. Energies of the rotational transitions, determined in the present experiments. Italic values denote transitions that were not previously reported.

Isotope	Energies of rotational transitions, keV $2^+\to 0^+$	$4^+\to 2^+$	$6^+\to 4^+$	$8^+\to 6^+$
Sm^{150}	335 ±3	450±5		
Sm^{152}	122 ±2	243±2	*337±5*	
Sm^{154}	82 ±1	186±2	*284±2*	*401±6*
Gd^{156}	88.5±1	200±2	300±3	*380±10*
Gd^{158}	79.5±1	183±2	282±3	
Gd^{160}	75 ±1	174±2	*265±2*	354±10
Dy^{162}	80 ±1	185±2	282±6	370±6
Dy^{164}	74 ±1	*169±2*	*258±2*	*332±8*
Er^{166}	81 ±1	183±3	278±4	
Er^{168}	80.5±1	185±2	282±4	
Er^{170}	79 ±1	180±2	*275±4*	
Yb^{172}	80 ±1	181±3	272±4	
Yb^{174}	76 ±1	*175±2*	*271±4*	*345±8*
Yb^{176}	82 ±1	187±2	*294±3*	*383±6*
Hf^{178}	94 ±1	217±3	328±9	
Hf^{180}	93 ±1	215±2	338±4	
W^{182}	101 ±1	229±3	350±4	
W^{184}	112 ±1	254±2		
W^{186}	122.5±1	276±3	*419±6*	
Os^{188}	155 ±3	325±6		
Os^{190}	188 ±3	360±15		
Os^{192}	205 ±2	380±10		

D. Results on Nonrotational Transitions

The excitations of the second 2^+ states in the nuclei Gd^{160}, W^{186}, Os^{188}, and Os^{192}, and of an excited $0'^+$ state in Sm^{152} (see Fig. 14) are analyzed on the basis of first- and second-order perturbation calculations. For the bombarding energies used in the present work,

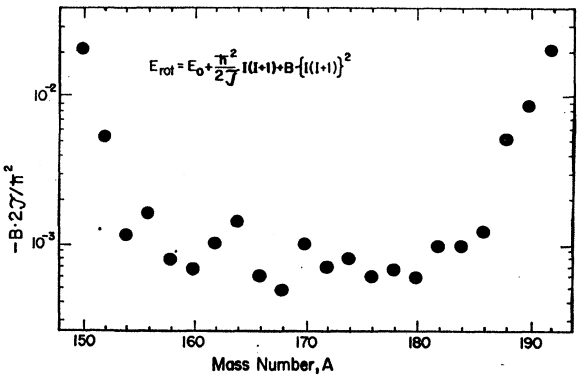

FIG. 12. The energy parameter $B\times 2\mathcal{J}/\hbar^2$ as a function of the mass number A. The parameter was not determined exclusively from the values of Table III but from an average of all data available.

[22] O. Hansen, M. C. Olesen, O. Skilbreid, and B. Elbek, Nucl. Phys. **25**, 634 (1961).
[23] B. Elbek, M. C. Olesen, and O. Skilbreid, Nucl. Phys. **19**, 523 (1960).
[24] D. B. Fossan and B. Herskind, Phys. Letters **2**, 155 (1962).

the $2'^+$ states are populated with about equal strength by the direct $E2$ excitation from the ground state and by the double $E2$ transition via the 2^+ rotational state. In second-order perturbation, the excitation probability contains three terms, corresponding to the two mentioned modes of excitation and the interference between the two.

The sign of the interference term depends on the relative sign of the reduced $E2$ matrix elements connecting the 0^+ and 2^+ states with the $2'^+$ state. It can in principle be determined by Coulomb-excitation experiments, if the excitation probability of the $2'^+$ state is measured for several bombarding energies. The perturbation analysis of the experiments then yields two sets of $B(E2)$ values for each choice of the sign of the interference term, and the decision between the two can be made by the requirement that the $B(E2)$ values of one set be equal for all bombarding energies.

The numerical formula, used in the analysis of the $2'^+$ excitation probabilities, is given by

$$P_{2'}=\chi_{0\to 2}^2\times\frac{B(E2,\,0\to 2')}{B(E2,\,0\to 2)}$$
$$\times[17.90\sin^4(\theta/2)df(\xi_{0\to 2'},\theta)/d\Omega$$
$$\pm 9.49\chi_{0\to 2}\times(\lambda(\Delta E_{2'\to 0}/\Delta E_{2'\to 2})^5)^{1/2}$$
$$\times\{\xi_{0\to 2'},\xi_{0\to 2},\xi_{2\to 2'},\theta\}$$
$$+16.03\chi_{0\to 2}^2\times\lambda(\Delta E_{2'\to 0}/\Delta E_{2'\to 2})^5$$
$$\times\sin^4(\theta/2)dF(\xi_{0\to 2'},\xi_{2\to 2'},2,\theta)/d\Omega]. \quad (18)$$

The quantities $df/d\Omega$ and $dF/d\Omega$ are tabulated in Refs. 1 and 21. The branching ratio λ is defined by

$$\lambda=\Gamma(E2,\,2'\to 2)/\Gamma(E2,\,2'\to 0), \quad (19)$$

where $\Gamma(E2)$ denotes the electric quadrupole gamma-ray transition probability. The sign of the second term

TABLE III. Summary of experimental results and comparison with theory. The number in parenthesis, following each experimental value, gives the relative error in percent.

1	2	3	4	5	6	7	8	9	10	11	12	13
				$B(E2)^d$	Experimental de-excitation probabilities R_I				$R_{I\,\mathrm{exp}}/R_{I\,\mathrm{theory}}$[e]			
Isotope	E_{0x}[a] MeV	ξ[b] $0\to 2$	χ[c] $0\to 2$	$0\to 2$ $e^2\times10^{-48}$ cm^4	$R_2\times10$	$R_4\times10^2$	$R_6\times10^3$	$R_8\times10^4$	$2\to 0$	$4\to 2$	$6\to 4$	$8\to 6$
Sm^{150}	34.8	0.284	0.357	1.30	0.50(15)	···	···	···	0.89			
	43.6	0.202	0.500		1.71(10)	0.89 (20)	···	···	1.27	2.0	···	···
Sm^{152}	29.9	0.130	0.470	3.43	1.45(12)	0.36 (22)	···	···	0.98	1.00	···	···
	39.0	0.087	0.700		···	2.38 (17)	0.59(40)	···	···	1.05	1.03	···
	43.1	0.075	0.820		···	4.27 (9)	2.48(15)	···	···	0.99	1.57	···
Sm^{154}	31.6	0.080	0.635	4.54	···	1.19 (10)	0.26(22)	···	···	0.77	0.97	···
	37.7	0.062	0.824		···	3.80 (9)	1.28(15)	0.36(50)	···	0.84	0.82	1.4
	41.5	0.053	0.952		···	5.79 (9)	3.06(15)	1.1 (40)	···	0.75	0.75	1.1
	41.5	0.053	0.952		5.09(10)	5.60 (10)	···	···	0.91	0.72	···	···
Gd^{156}	34.8	0.077	0.629	4.50	3.48(10)	1.59 (11)	···	···	1.22	1.04	···	···
	40.3	0.062	0.784		···	4.39 (9)	1.75(25)	···	···	1.15	1.42	···
	43.8	0.055	0.890		···	6.31 (8)	3.57(15)	1.3 (35)	···	1.02	1.30	2.0
Gd^{158}	34.8	0.069	0.687	5.36	3.70(10)	2.04 (11)	···	···	1.11	0.92	···	···
	36.9	0.064	0.752		···	2.92 (9)	0.94(15)	···	···	0.91	1.03	···
	40.3	0.056	0.858		···	5.18 (9)	2.13(15)	···	···	0.88	1.00	···
Gd^{160}	33.9	0.068	0.718	5.71	···	1.99 (10)	0.50(22)	···	···	0.76	0.76	···
	39.1	0.054	0.892		5.07(9)	4.09 (10)	···	···	1.00	0.66	···	···
	39.1	0.054	0.892		···	4.67 (10)	1.92(18)	···	···	0.75	0.71	···
	42.0	0.049	0.993		···	7.10 (10)	3.87(17)	···	···	0.77	0.74	···
	43.9	0.046	1.060		···	8.83 (8)	5.20(15)	3.4 (50)	···	0.76	0.65	1.3
Dy^{162}	34.6	0.072	0.630	5.03	2.92(11)	1.77 (9)	0.17(50)	···	1.02	1.14	0.60	···
	41.5	0.055	0.819		···	5.05 (10)	2.20(30)	0.4 (60)	···	1.10	1.34	1.3
Dy^{164}	34.9	0.066	0.667	5.55	3.68(11)	2.15 (11)	···	···	1.15	1.04	···	···
	41.6	0.051	0.864		···	6.52 (10)	2.35(26)	1.5 (50)	···	1.14	1.01	2.8
Er^{166}	34.9	0.074	0.634	5.58	3.23(11)	1.76 (11)	···	···	1.04	0.98	···	···
	41.5	0.055	0.815		···	4.98 (10)	1.63(22)	···	···	1.10	1.04	···
Er^{168}	34.8	0.074	0.634	5.64	3.21(11)	1.90 (11)	···	···	1.11	1.19	···	···
	41.5	0.055	0.822		···	4.50 (11)	1.49(32)	···	···	0.97	0.87	···
Er^{170}	34.8	0.072	0.617	5.35	3.36(12)	1.82 (12)	···	···	1.22	1.13	···	···
	34.8	0.072	0.617		···	1.98 (11)	0.37(40)	···	···	1.23	1.40	···
	41.7	0.054	0.809		···	5.19 (10)	1.96(22)	···	···	1.18	1.25	···

TABLE III. (*Continued*).

1	2	3	4	5	6	7	8	9	10	11	12	13
				$B(E2)^{d}$	Experimental de-excitation probabilities R_I				$R_{I\,\mathrm{exp}}/R_{I\,\mathrm{theory}}{}^{e}$			
Isotope	$E_{0x}{}^{a}$ MeV	ξ^{b} $0\to2$	χ^{c} $0\to2$	$0\to2$ $e^2\times10^{-48}$ cm^4	$R_2\times10$	$R_4\times10^2$	$R_6\times10^3$	$R_8\times10^4$	$2\to0$	$4\to2$	$6\to4$	$8\to6$
Yb^{172}	34.8	0.077	0.608	5.80	3.02(11)	1.60 (11)	···	···	1.13	1.15	···	···
	41.6	0.058	0.792		···	4.21 (9)	1.51(22)	···	···	1.04	1.12	···
Yb^{174}	34.7	0.072	0.607	5.80	3.15(11)	1.51 (11)	···	···	1.18	1.10	···	···
	38.8	0.061	0.717		···	3.06 (10)	0.81(22)	···	···	1.10	1.14	···
	41.5	0.055	0.791		···	4.19 (9)	1.58(17)	0.5 (60)	···	1.03	1.15	2.0
Yb^{176}	34.7	0.077	0.602	5.69	2.94(10)	1.37 (9)	···	···	1.13	1.06	···	···
	34.7	0.077	0.602		···	1.44 (9)	0.17(31)	···	···	1.11	0.85	···
	41.6	0.059	0.790		···	3.88 (9)	1.29(22)	0.6 (50)	···	0.98	1.03	2.8
Hf^{178}	34.8	0.091	0.521	4.66	2.19(11)	0.78 (12)	···	···	1.14	1.20	···	···
	40.4	0.073	0.625		···	2.07 (9)	0.68(32)	···	···	1.36	2.56	···
Hf^{180}	34.9	0.090	0.502	4.30	2.25(11)	0.71 (12)	···	···	1.24	1.25	···	···
	38.1	0.079	0.572		···	1.26 (9)	0.30(32)	···	···	1.21	2.07	···
	41.2	0.070	0.644		···	2.26 (10)	0.60(50)	···	···	1.28	1.85	···
W^{182}	34.2	0.103	0.451	4.10	1.72(11)	0.48 (11)	···	···	1.18	1.42	···	···
	41.5	0.077	0.600		···	1.23 (17)	0.32(35)	···	···	0.96	1.56	···
	43.0	0.073	0.633		···	1.66 (12)	0.19(50)	···	···	1.04	0.64	···
W^{184}	34.7	0.112	0.441	3.74	1.64(10)	0.35 (12)	···	···	1.20	1.10	···	···
	37.9	0.099	0.503		···	0.73 (11)	···	···	···	1.34	···	···
W^{186}	28.0	0.167	0.304	3.40	0.73(13)	0.025(35)	···	···	1.19	0.62	···	···
	43.8	0.086	0.594		···	1.40 (11)	0.41(60)	···	···	1.23	2.3	···
Os^{188}	43.3	0.113	0.463[f]	3.1[f]	1.49(17)	0.44 (36)	···	···	1.00[f]	1.20	···	···
	43.8	0.112	0.455[f]		1.44(12)	0.51 (30)	···	···	1.00[f]	1.48	···	···
Os^{190}	43.8	0.135	0.414[f]	2.5[f]	1.15(22)	0.48 (50)	···	···	1.00[f]	2.18	···	···
Os^{192}	43.8	0.148	0.414[f]	2.5[f]	1.12(17)	0.20 (40)	···	···	1.00[f]	0.98	···	···

[a] Corrected for energy loss in the target.
[b] Adiabaticity parameter, defined in Eq. (10).
[c] Transition amplitude for the $0^+\to2^+$ excitation in first order perturbation ($\xi=0$ and $\theta=180°$).
[d] Values taken from Refs. 22 and 23.
[e] $R_{I\,\mathrm{theory}}$ was determined for a moment of inertia which reproduces the energy of the transition $I\to I-2$.
[f] For the osmium isotopes $B(E2,\,0\to2)$ values determined by inelastic scattering experiments, are not available. The quoted values are adjusted in such a way as to make $R_{2\,\mathrm{exp}}/R_{2\,\mathrm{theor}}=1.00$.

in the square brackets of Eq. (18) is the same as the relative sign of the two reduced matrix elements $\langle 2'||E2||0\rangle$ and $\langle 2'||E2||2\rangle$. The curly bracket in the second term in defined as

$$\{\xi_{0\to2'},\xi_{0\to2},\xi_{2\to2'},\theta\}=(\tfrac{3}{2})^{1/2}[I_{22}(\cdots)\times\beta_{2-2}(\cdots)+I_{2-2}(\cdots)\times\beta_{22}(\cdots)]-I_{20}(\cdots)\beta_{20}(\cdots). \quad (20)$$

The arguments of $I_{2\mu}(\cdots)$ in Eq. (20) are $(\xi_{0\to2'},\theta)$, and of $\beta_{2\kappa}(\cdots)$ they are $(2,2,\xi_{0\to2},\xi_{2\to2'},\theta)$. The functions $I_{2\mu}$ and $\beta_{2\kappa}$ are tabulated in Refs. 1 and 21, respectively.

In Sm^{152}, a $0'^+$ level at 685 keV was excited by double Coulomb excitation. The numerical formula for the excitation probability is for this case

$$P_{0'}{}^{(22)}=4.48\chi_{0\to2}{}^{4}\times\frac{B(E2,\,2\to0')}{B(E2,\,0\to2)}\times\sin^4(\theta/2)dF(\xi_{0\to2},\xi_{2\to0'},0,\theta)/d\Omega. \quad (21)$$

The results on the excitation of nonrotational levels and the $B(E2)$ values extracted from the experimental excitation probabilities are summarized in Table IV. The number in parenthesis following each experimental quantity gives its relative error in percent. The relative errors in the $B(E2)$ values are the same as in the excitation probabilities. The multipolarity of the $2'^+\to2^+$ transition has been assumed to be pure $E2$, the $M1$ contributions being in most cases smaller than 2%.[25] For the de-excitation of the $2'^+$ states, two sets of $B(E2)$ values are given, corresponding to the two signs of the interference term in Eq. (18). The relative sign of the reduced matrix elements, which was used in the determination of the $B(E2)$ values, is indicated in parenthesis following the experimental number for $B(E2)$. In the case of Gd^{160}, where the excitation of the 1010-keV state was observed at two bombarding energies, the experimental accuracy is not sufficient to allow a decision between the two signs. In the nuclei W^{186}, Os^{188}, and Os^{112}, the interference term is so small that the two sets of $B(E2)'$s are almost equal. The

[25] F. K. McGowan and P. H. Stelson, Phys. Rev. **122**, 1274 (1961).

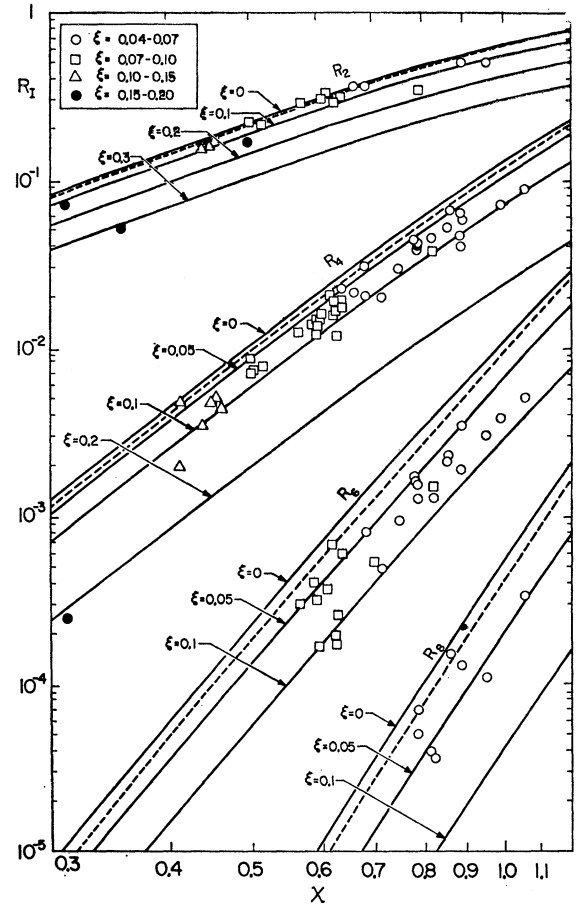

FIG. 13. De-excitation probabilities R_I as a function of χ and ξ. The solid curves represent $R_I(\chi, \xi, \theta=180°)$, calculated in Ref. 3 and the dashed lines show $R_I(\chi, \xi=0, \theta=160°)$ from Ref. 4. The experimental points are plotted for the $\chi_{0\to2}$ and $\xi_{0\to2}$ values quoted in Table IV.

$B(E2)$ values, reported in the present paper, are in fair agreement with the ones quoted in Ref. 25. In all cases, our values are somewhat smaller.

V. DISCUSSION

The aim of the present experiments was to study in detail the multiple Coulomb excitation of the ground-state rotational bands in deformed even-even nuclei. In the experiments some transitions to other states were also observed.

A. Rotational Transitions

As was shown in Sec. IIIC, the perturbation treatment fails to describe the excitation of the ground-state rotational bands under the bombarding conditions of the present experiments. A realistic description of the process must take into account a large number of nuclear quantities which can not be determined independently from the measured excitation probabilities. Instead we have compared our results with a calculation for a pure rotational band[3] and a good agreement has been found (cf. Figs. 5, 6, and 13). We believe, however, that the accuracy of the experiments allows one to interpret the small deviations from the calculations in terms of small deviations from the pure rotational description. The effects arising from the deviations of the energies from the $I(I+1)$ rule are discussed in Sec. IVB. In the following it is attempted to interpret the remaining discrepancies in terms of a variation of the intrinsic quadrupole moment Q_0.

We can best illustrate this approximative procedure by an example: In lowest order perturbation (l.o.p.), R_2 depends only on $B(E2, 0\to2)$ and R_4 depends only on the product $B(E2, 0\to2)\times B(E2, 2\to4)$, so that $(R_4/R_2)_{\text{l.o.p.}} \propto B(E2, 2\to4)$. We now calculate $R_4^{(\text{l.o.p.})}/$

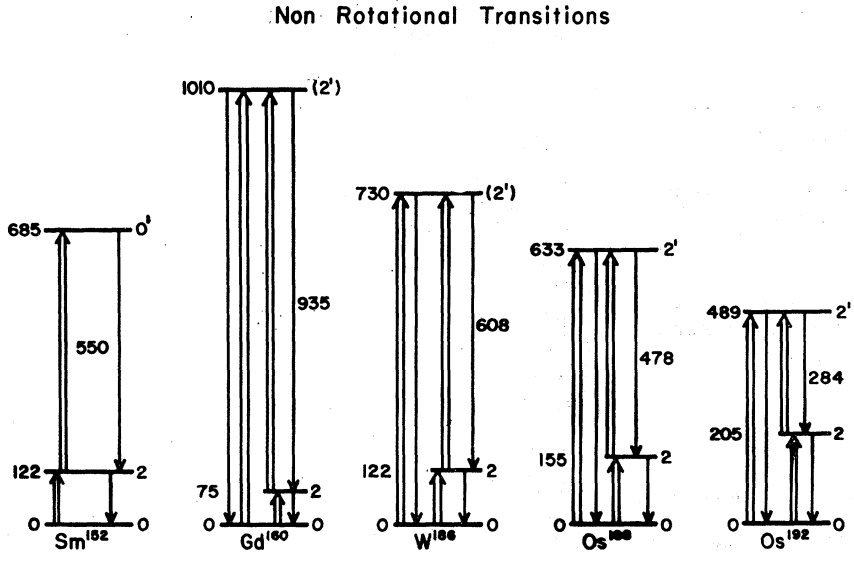

FIG. 14. Level diagrams, depicting the nonrotational transitions observed in the present experiments.

TABLE IV. Results on the excitation of nonrotational levels. The numbers in parenthesis, following each experimental figure, are the relative errors in percent. The plus (or minus) sign following the $B(E2)$ values denotes that the two reduced $E2$-matrix elements connecting the $2'^{+}$ state with the 2^{+} and 0^{+} rotational states have the same (or the opposite) sign.

Isotope	E_{0x} MeV	E_γ keV	Level energy keV	Assignment of decay	Branching ratio ($E2$) $\frac{2'\to 2}{2'\to 0}$	Excitation probability 10^{-3}	$B(E2)$ for de-excitation $e^2\times10^{-48}$ cm^4
Sm^{152}	39.0	550±15	685	$0'\to 2^a$	···	0.6(30)	1.9
	43.1	550±15	685	$0'\to 2^a$	···	1.7(25)	2.5
Gd^{160}	39.1	1010±15	1010	$2'\to 0$	1.6(30)	1.3(40)	0.026(−); 0.015(+)
		930±15	1010	$2'\to 2$			0.060(−); 0.035(+)
	43.9	1010±15	1010	$2'\to 0$	1.4(30)	2.9(35)	0.020(−); 0.013(+)
		930±15	1010	$2'\to 2$			0.046(−); 0.030(+)
W^{186}	43.8	732±10	730	$2'\to 0^b$	0.73(25)	3.1(30)	0.019(−); 0.017(+)
		605±10	730	$2'\to 2^b$			0.035(−); 0.032(+)
Os^{188}	43.8	640±10	633	$2'\to 0^b$	0.68(25)	6.4(30)	0.030(−); 0.028(+)
		475±10	633	$2'\to 2^b$			0.083(−); 0.077(+)
Os^{192}	43.8	495±10	489	$2'\to 0^b$	0.57(30)	6.9(40)	0.013(−); 0.012(+)
		285±10	489	$2'\to 2^b$			0.11(−); 0.10(+)

[a] Assignment taken from Ref. 27 and 28.
[b] Assignments taken from Ref. 25.

$R_2^{(\text{l.o.p.})}$ with $B(E2,\ 2\to 4)_{\text{theor}}$ given by Eq. (2), whereby Q_0 is taken from Refs. 22 and 23. In l.o.p. we have

$$(R_4/R_2)_{\text{exp}}/(R_4/R_2)_{\text{l.o.p.}} = B(E2,\ 2\to 4)_{\text{exp}}/B(E2,\ 2\to 4)_{\text{theor}}. \quad (22)$$

The proportionality between (R_4/R_2) and $B(E2,\ 2\to 4)$ does no longer hold exactly, if higher than lowest order terms are included in the calculations. We can, however, estimate the effect of the inclusion of higher order terms by comparing R_4/R_2 for the lowest order perturbation calculations with the value of the calculation of Ref. 3. This comparison is illustrated in Fig. 15. The de-excitation probabilities R_2 and R_4 are calculated for a symmetric rotator by the diagonalization method[3] (solid lines) and in l.o.p. (broken lines). In the doubly logarithmic plot, the first- and second-order perturbation calculations give straight lines with slopes of χ^2 and χ^4, respectively. It can be seen from the calculated curves that, in the range of χ and ξ encountered in the present experiments, the ratios R_4/R_2 are indeed very closely the same for the perturbation calculations and for the diagonalization method. If we now assume that corresponding relations also hold for higher excitations, we can write for the double ratios

$$D_I\equiv\frac{(R_I/R_{I-2})_{\text{exp}}}{(R_I/R_{I-2})_{\text{diag. method}}} \approx\frac{(R_I/R_{I-2})_{\text{exp}}}{(R_I/R_{I-2})_{\text{l.o.p.}}}\approx\frac{B(E2,\ I-2\to I)_{\text{exp}}}{B(E2,\ I-2\to I)_{\text{theor}}}. \quad (23)$$

The double ratios D_I, calculated for Q_0-values of Refs. 22 and 23, are plotted in Fig. 16 for $I=4$, 6 and 8, as a function of the mass number A. The experimental points lie fairly close to a line corresponding to $D_I=1$ which indicates that the intrinsic quadrupole moment Q_0 is to a good approximation a constant for all transitions within the ground state rotational band. Li and Schwarzschild[6] came to the same conclusion from their measurements of the lifetimes of 2^+ and 4^+ states of strongly deformed nuclei. The present measurements, however, show a slight increase of D_I for nuclei in the transition region, where Q_0 is smaller than in the region of strong deformation. Also, the deviation of D_I to values greater than 1 is more pronounced for the higher rotational states. These observations are in

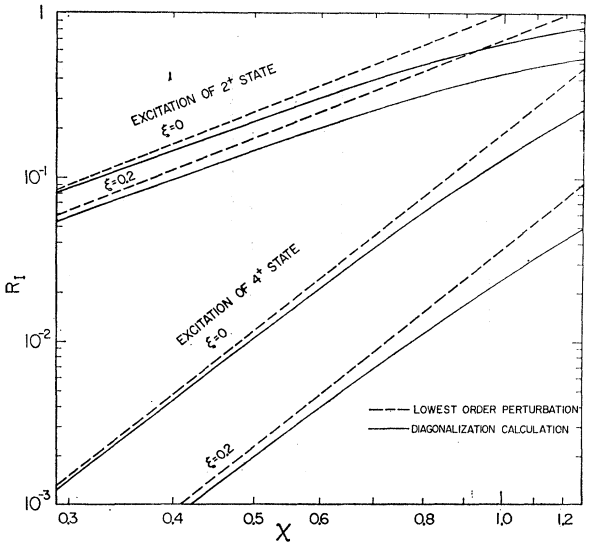

FIG. 15. Comparison of the calculations in Ref. 3 of the multiple Coulomb excitation of a symmetric rotator with lowest order perturbation calculations (first order for the excitation of the 2^+ state, second order for the 4^+ state). In the doubly logarithmic plot, the perturbation calculations are straight lines with slopes corresponding to χ^2 for first-order and χ^4 for second-order perturbation.

TABLE V. Comparison of the $B(E2)$ ratios with the predictions of the asymmetric-rotator model by Davydov *et al.* (Ref. 9).

Isotope	$B(E2, 2' \rightarrow 2)/B(E2, 2 \rightarrow 0)$ Experiment	Theory	$B(E2, 2' \rightarrow 0)/B(E2, 2 \rightarrow 0)$ Experiment	Theory	$B(E2, 2' \rightarrow 2)/B(E2, 2' \rightarrow 0)$ Experiment	Theory
Gd^{160}	0.053±0.016	0.064	0.023±0.007	0.031	2.3±0.5	1.78
W^{186}	0.051±0.015	0.18	0.028±0.009	0.061	1.9±0.4	3.05
Os^{188}	0.13 ±0.04	0.32	0.048±0.014	0.071	2.2±0.6	4.60
Os^{192}	0.22 ±0.09	0.94	0.026±0.008	0.042	8.6±1.7	23.5

qualitative agreement with the fact that the moment of inertia becomes larger with higher spin[26] and that its relative change increases at the border of the region of strong deformations (see Fig. 11). A quantitative treatment would require the inclusion of nuclear degrees of freedom in addition to those of a symmetric top.

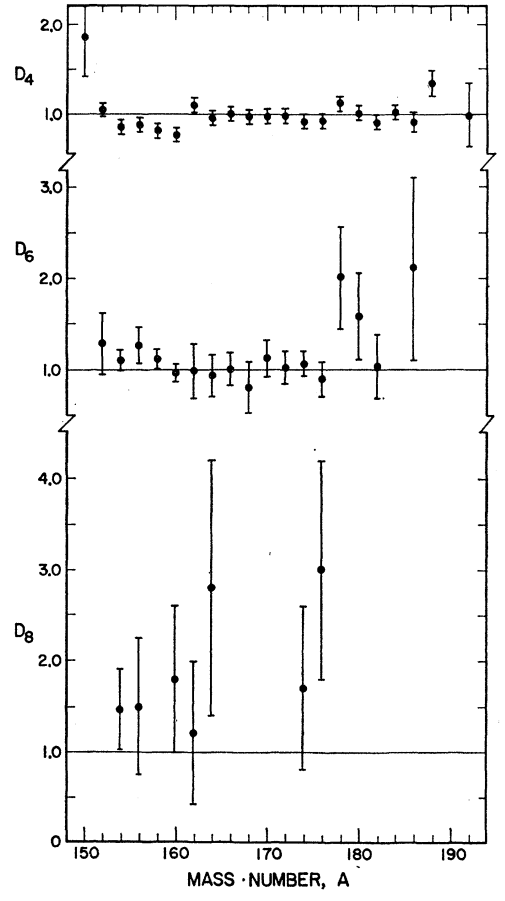

FIG. 16. The quantities D_I, defined as $(R_I/R_{I-2})_{\text{exp}}$: $(R_I/R_{I-2})_{\text{diag. method}}$ are plotted for $I=4$, 6, and 8 as a function of the mass number A. In an approximative way (see text), the deviation of D_I from 1 is proportional to the deviation of $B(E2, I \rightarrow I-2)/B(E2, 2 \rightarrow 0)$ from the value predicted by the symmetric-rotator model [Eq. (2)].

[26] H. Morinaga and P. C. Gugelot, Nucl. Phys. **46**, 210 (1963).

B. Nonrotational Transitions

An excited $0'^+$ state in Sm^{152} has been observed in the decay of Eu^{152} by Marklund *et al.*[27] and in Coulomb-excitation experiments by Greenberg *et al.*[28] The assignment of the 550±15-keV gamma ray as a $0'^+ \rightarrow 2^+$ transition is based on the work of these authors. Our experiments, however, do not show a gamma ray of about 690 keV, which is reported in Ref. 28. The intensity of this line is, according to Ref. 28, about equal to the intensity of the $0'^+ \rightarrow 2^+$ transition, and and the line should therefore have been observed in the present investigations.[29]

The nature of the $2'^+$ states has been extensively discussed by McGowan and Stelson.[25] In analogy with these authors, we present in Table V a comparison of our results for the ratios of $B(E2)$ values with the asymmetric rotator model of Davydov and Filippov.[9] For this comparison, the sign of the interference term has been chosen in such a way as to give the best agreement with Ref. 9. In each case, this leads to the assumption that the two matrix elements connecting the $2'^+$ state with the 2^+ and 0^+ rotational states have opposite sign. The agreement of our values with the model of Davydov and Filippov is in most cases not as good as the agreement obtained by McGowan and Stelson.[25,30]

ACKNOWLEDGMENTS

The authors want to thank Dr. Zeev Vager and Yacov Dar at the Weizmann Institute of Science for the preparation of some of the targets used in these experiments. We are most grateful to Clyde Zaidins for his assistance during the measurements. We are indebted to Dr. K. Alder, D. Beder, Dr. F. Boehm, Dr. J. Eichler, Dr. T. Lauritsen, and Dr. A. Winther for many valuable discussions. It was of great help to us that Dr. K. Alder made the results of his calculations available prior to their publication.

[27] I. Marklund, O. Nathan, and O. B. Nielsen, Nucl. Phys. **15**, 199 (1960).

[28] J. S. Greenberg, G. G. Seaman, E. V. Bishop, and D. A. Bromley, Phys. Rev. Letters **11**, 211 (1963).

[29] *Note added in proof.* The relative intensity of the 690 keV line was found to be much higher in the *direct* gamma spectrum than in coincidence with *backscattered* particles [J. S. Greenberg (private communication)].

[30] *Note added in proof.* The work of Lutken and Winther shows that the perturbation treatment might not be adequate in this case (to be published in Kgl. Danske Videnskab. Selskab, Mat. Fys. Medd.).